Aerosol Deposited BaTiO3 Film Based Interdigital Capacitor and Squared Spiral Capacitor for Humidity Sensing Application

Journal:	*Inorganic Chemistry*
Manuscript ID	ic-2020-01580w
Manuscript Type:	Article
Date Submitted by the Author:	29-May-2020
Complete List of Authors:	Kumar, Alok; Harbin Institute of Technology, Wang, Cong ; Harbin Institute of Technology School of Electronics and Information Engineering Meng, Fan-Yi ; Harbin Institute of Technology Liang, Jun-Ge ; Jiangnan University Xie, Bing-Fang ; Harbin Institute of Technology Zhou, Zhong-Liang ; Harbin Institute of Technology Zhao, Meng ; Suzhou University of Science and Technology Kim, Nam-Young ; Kwangwoon University

Aerosol Deposited $BaTiO_3$ Film Based Interdigital Capacitor and Squared Spiral Capacitor for Humidity Sensing Application

Alok Kumar[a], Cong Wang*[a], Fan-Yi Meng[a], Jun-Ge Liang*[b], Bing-Fang Xie[a], Zhong-Liang Zhou[a], Meng Zhao[c], and Nam-Young Kim*[d]

[a]School of Information and Communication, Harbin Institute of Technology, Harbin, China
[b]Department of Electronic Engineering, Jiangnan University, Wuxi 214122, China
[c]School of Mathematics and Physics, Suzhou University of Science and Technology, Suzhou, China
[d]Department of Electronic Engineering, Kwangwoon University, Seoul 139701, Republic of Korea

kevinwang@hit.edu.cn, (C. Wang), jgliang@jiangnan.edu.cn (J.-G. Liang), nykim@kw.ac.kr(N.-Y. Kim)

Abstract: In this article, ultra-high sensitive aerosol deposited BaTiO3 film based inter-digital capacitors (IDCs), and a squared spiral capacitor (SSC) have been investigated for humidity sensing application. BaTiO3 based sensing film is prepared at room temperature, then post-annealed at 200 ºC and 400 ºC to enhance material's sensing properties. Thermal exposure of BaTiO3 sensing film increases electron density, improves material defects, enhances grain to grain connectivity, and escalates hydrophilicity. The sensitivity of all fabricated devices is evaluated by comparing capacitive variation at different relative humidity (RH) levels. The electric field distribution and open area ratio (OAR) are scrutinized to understand the effect of these parameters on the humidity sensing mechanism. The obtained results indicate IDC-1 with large OAR reveals high sensitivity due to the availability of a wider interaction area for fringing electric field intensity and water vapours adsorbed on sensing material surface. Similarly, the SSC structure reveals high sensitivity over IDC-2 and IDC-3 due to existence of concentrated electric field intensity and large OAR. The high electric field intensity polarizes the water vapour molecules and sensing material ions that upsurge device capacitance at various RH levels, thus enhance sensitivity. The current study reveals that the design structure, electric field intensity and sensing material property are equally responsible for high sensitivity in capacitive humidity sensors.

Introduction

Humidity sensors play a significant role in environmental control, industrial processing, agriculture production, grain storage, and medical processes. These sensors generate an electrical signal in accordance with the change in relative humidity content present in the surrounding environment. The practical humidity sensors must have fast response, good linearity, high sensitivity, low hysteresis, and long-term operational stability.[1] Recently, several resistive type, a capacitive type, field-effect transistor type, and microwave type humidity sensors have been reported for practical applications.[2,3]

Capacitive humidity sensors present high sensitivity, low fabrication cost, fast response, ease of integration, and low energy consumption.[4] In capacitive sensors, inter-digital capacitive structures are prevalent due to their coplanar arrangements that lead to ease in fabrication and integration. Recent advancement of the micro-fabrication process also benefits the coplanar designs to achieve a higher degree of miniaturization and large scale integration. The electrode size and space of inter-digital structures can be adjusted up to a few microns through the advanced micro-fabrication process on which the sensing material can be deposited precisely to achieve high sensitivity.[5] The overall capacitance of inter-digital capacitive structures mainly depends upon the electrode surface conductivity (σ) and the effective dielectric constant (ε) of the sensing material present between the adjacent charge electrodes.[6,7] Also, the humidity sensing analysis of these capacitive structures is promoted by the variation of σ and ε in the sensing area. The presence of sensing material and optimum design structure help to enhance the selectivity, sensitivity, chemical and thermal stability of capacitive humidity sensors.[8]

Ceramic materials are a prominent choice for sensing materials because of high thermal, chemical and physical stability.[9] They have a high-roughness surface that makes them more susceptible to water vapours. However, barium titanate ($BaTiO_3$) is a promising ceramic material for humidity sensing application due to its high dielectric constant, lead-free and eco-friendly properties.[10] $BaTiO_3$ has a perovskite-type structure with a general stoichiometry of ABO_3, where A (Ba) represents alkaline material which is highly sensitive to water vapours, B (Ti) represents ferroelectric material which is responsible for high dielectric constant and O represent oxygen element. This structural formation is responsible for Grotthus chain reaction in a humid environment.[11] Various studies have been carried out for the preparation of $BaTiO_3$ sensing films such as wet chemical method, solid-state sintering, stearic acid-gel method, electro-spinning, and sol-gel method etcetera.[9,12,13] But all these methods require high annealing/sintering temperature to enhance crystallization effects. Recently, aerosol-deposition (AD) method is introduced to prepare porous ceramic film through direct deposition at room temperature.[14]

$BaTiO_3$ based inter-digital structures are already explored for humidity sensing analysis [9,15,16,] but the effect of design structure and electric field intensity on humidity sensing is still obscure. The humidity sensing property of $BaTiO_3$ loaded inter-

digital structure can be influenced by high electric field intensity and device geometry. Therefore, the selection of optimized device structure and the effect of concentrated electric field intensity are crucial to examine for humidity sensing analysis.[17,18] The capacitance of sensing material depends on the complex effective permittivity and the gap between adjacent charge electrodes.[19] Although, the presence of small gap increases the overall device capacitance but also reduces the electric field penetration area inside the deposited sensing material.[20] The gap between the adjacent charge electrodes decides the interaction area between electric field intensity and deposited water vapours on the sensing material surface. This interaction affects the device capacitance by varying the surface conductivity (σ) and complex effective permittivity (ε) of sensing material. The concentrated electric field lines also affect the ferroelectric property of deposited $BaTiO_3$ material and vary its overall effective permittivity.[21] $BaTiO_3$ material is insoluble in water; hence, no electric field shielding is provided for the water vapours ions present on sensing material surface.[22] The electric field intensity strongly interacts with water vapour adsorption sites and dissociates the water ions to generate protonation. The formed protonation affects the overall conductivity of deposited sensing material. In a humid environment, when a strong external electric field interacts with $BaTiO_3$ material, it polarizes the isolated ferroelectric particles along with water vapour ions to encourage intense electric dipole moment that varies the effective permittivity of sensing material.[23] Therefore, it is essential to scrutinize the effect of open area ratio (OAR) and electric field intensity on humidity sensing through structural variation.

In this paper, the effect of design structure (OAR) and electric field intensity on humidity sensing is demonstrated by comparing the capacitive variation of different inter-digital structures. The OAR and electric field distribution are analyzed to strengthen the study with in-depth analysis. Moreover, three inter-digital capacitors (IDCs) and one squared spiral capacitor (SSC) are fabricated using advanced semiconductor fabrication technology to attain low profile structures. The fabricated devices are also embedded with aerosol deposited $BaTiO_3$ film prepared at room temperature and then annealed at 200 ºC, and 400 ºC, respectively to enhance device sensitivity. $BaTiO_3$ sensing film is deposited on the glass substrate using the AD method at room temperature. The $BaTiO_3$ film thickness of around 1.5 µm and 3.0 µm is a better choice to achieve high sensitivity but at a low relative humidity (RH) points the performance of 1.5 µm $BaTiO_3$ film far better than 3.0 µm $BaTiO_3$ film. The enhancement of sensitivity at low RH points is due to the existence of high open-pore ratio. Moreover, the film thickness of 1.5 µm attributes short response and recovery time [16] In our current study, the thickness of $BaTiO_3$ sensing film is fixed at 1.5 µm to achieve an ultra-high sensitivity with quick response and recovery time.

Experimental Methods

Sensing Film Preparation

The $BaTiO_3$ aerosol is deposited on fabricated sensors through shock load solidification mechanism at room temperature (Scheme 1). In this process, small particles of $BaTiO_3$ aerosol are accelerated with high pressure and bombarded on a glass substrate to form sensing film. First, the lighter gas helium present in the carrier gas cylinder is passed through a mass flow controller and insert in the aerosol chamber with high velocity. The aerosol chamber is placed on the top of vibratory equipment. The purpose of vibratory equipment is to convert preliminary granular powder of $BaTiO_3$ material from static solid-state to dynamic loose powder. The aerosol chamber contains high pressure which is generated via highly pressurized helium gas whereas, deposition chamber contains low pressure or vacuum which is created via a vacuum generator. This pressure difference accelerates aerosolized $BaTiO_3$ particles with high velocity from the aerosol chamber to the deposition chamber through a narrow sized nozzle. A filter is placed between the aerosol chamber and disposition chamber to filter-out large $BaTiO_3$ particles and passes desired particles to create uniformity. The fabricated sensor designs on the glass substrate are placed at the substrate holder, and the position of the holder can be adjusted through axis rotators.

In this experiment, 1.5 µm thick $BaTiO_3$ film is deposited over the glass substrate. This accurate thickness is achieved by fixing nozzle aperture at 10 × 0.4 mm^2, scanning speed of around 120 mm/min, and glass substrate to nozzle distance at 7 mm. The working pressure and temperature are set to 675 Pascal and 25~27 ºC, respectively. The parameters used to deposit high-quality $BaTiO_3$ sensing film are shown in Table S1. The bombarding of $BaTiO_3$ particles on the hard substrate generates a film with non-uniformed internal structure, distorted crystal lattice and high residual stress.[16] Post annealing was proved an effective solution to create uniform capillary microstructure with improved crystallinity and minimum residual stress.[24] In this research, the effect of temperature on humidity sensing analysis is also analyzed to obtain high sensitivity. The demonstrated $BaTiO_3$ sensing film is prepared at room temperature, then annealed at 200 ºC and 400 ºC. The annealing temperature of the pipe furnace is varied by 5 ºC per min in every cycle for two hours to avoid cracks on the deposited material.

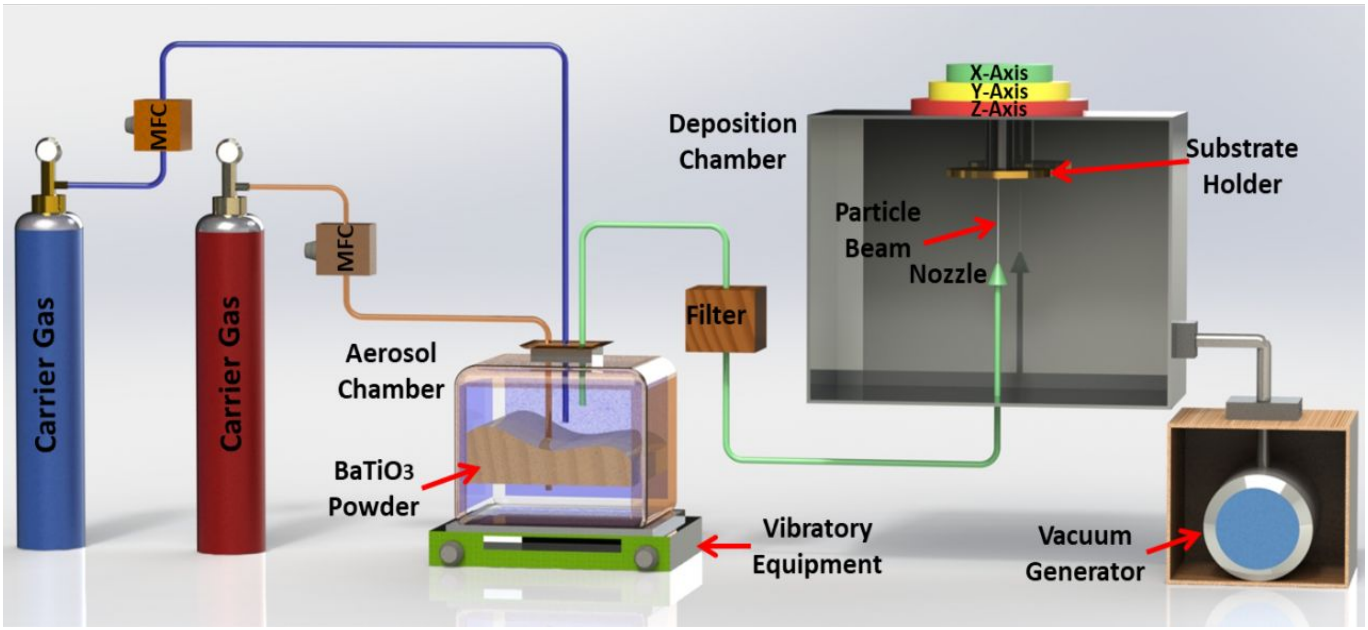

Scheme. 1. 3-D schematic of $BaTiO_3$ aerosol-based hygroscopic film fabrication

Sample Characterization

The structural formation of aerosol deposited $BaTiO_3$ film is evaluated by transmission electron microscopy (TEM), atomic force microscopy (AFM) and X-ray diffraction (XRD). TEM (JEM-2100F, JEOL) imaging is performed to extract the grain density of sensing film at different layers and to identify the formation of grain voids after thermal exposure. The AFM (XE150, PSIA) imaging is used to analyze the 3-D surface morphology of $BaTiO_3$ film prepared at different temperatures. The AFM data is analyzed by park System Corporation (XEI) software to get accurate surface roughness. Similarly, the crystalline property and average crystallite size of prepared material are evaluated by XRD (ATX-G, Rigaku Co., Japan) measurement. The material scanning is executed at 20° - 70° with a scanning rate of 2°/min. The XRD characterization is done by MDI Jade 6 and Origin Pro 8. Scherrer theorem is used to approximate the crystallite size of prepared material and annealed at different temperatures:-

$$\boldsymbol{D} = \frac{\boldsymbol{k\lambda}}{\boldsymbol{\beta \cos \theta}} \quad (1)$$

Where *D* represents crystallite size, *k* represents dimensionless shape factor, *λ* represents X-Ray wavelength, *β* represents full width at half maximum, and *θ* represents Bragg angle.

Device Preparation

Four different inter-digital structures are fabricated and analyzed for humidity sensing application. Three IDCs with different finger gap and one squared spiral capacitor (SSC) are designed and simulated using Agilent Advanced Design System (ADS) 2016 software and later fabricated through advanced fabrication technology on the glass substrate.

The isolation of three IDCs and one SSC is done on the basis of the number of electrodes (*N*), finger width (*WF*), finger length (*FL*), finger gap (*GF*), gap between the electrode and feed line (*GFE*), and feed line width (*WL*). The 3-D schematic, dimension marker and equivalent circuit of the proposed structure on glass substrate are shown in Figures 1(a, b, c and d). The equivalent circuit of IDC and SSC represents the series/parallel combination of inductor and capacitor that equivalent to electrodes conductive path and the gap between them. In the presented equivalent structure, *L* represents inductance, C_g represents gap capacitance, and C_c represents coupling capacitance. The coupling capacitance of IDC can be expressed as.[25]

$$C_c = 4\varepsilon_0 \varepsilon^*_{sm} \times \frac{K(K')}{K(K)} \text{ pF/cm} \quad (2)$$

$$K = \left(1 + \frac{2 \times WF}{2 \times GF + WF}\right) \times \left(\sqrt{\frac{1}{1 + \frac{2 \times WF}{GF}}}\right) \quad (3)$$

$$K' = \sqrt{1 - K^2} \quad (4)$$

Whereas, the overall capacitance of the IDC structure can be represented as

$$C_{IDC} = \left[\varepsilon^*_{sm}\varepsilon_0\left(\frac{1+\varepsilon_s}{2}\right) \times \frac{K(\sqrt{1+K^2})}{K(k)} + \varepsilon_s\varepsilon_0\frac{WF}{GF}\right] \times (N-1)LF \quad (5)$$

Where, ε^*_{sm} represents complex permittivity of sensing material present on electrodes (in case of air ε^*_{sm}= 1), ε_0 represents effective permittivity of free space ($\varepsilon_0 = 8.854 \times 10^{-12} F/m$), ε_s represents substrate permittivity, *K* represents first elliptical integral, *k* represents the ratio of finger width and finger gap (*WF/GF*), *N* represents the number of electrodes, and *LF* represents the length of electrode finger. In conventional SSC models, gap capacitance (C_g) was considered as an important factor to decide overall device capacitance. But, after the advancement of advanced microfabrication techniques

coupling capacitance (C_c) become a significant parameter for capacitive variation.[26] The overall circuit capacitance of SSC can be represented as.[27]

$$C_{SSC} = \left[\varepsilon^*_{sm}\varepsilon_0\left(\frac{1+\varepsilon_s}{2}\right) \times \frac{K(\sqrt{1+K^2})}{K(k)} + \varepsilon_s\varepsilon_0\frac{WF}{GF}\right] \times LF \quad (6)$$

Eqs 5 and 6 represent the effective device capacitance is directly proportional to the complex permittivity of sensing material. In a humid environment, the available water vapours content vary the complex permittivity of sensing material that correspondingly alter the overall device capacitance. The physical parameter of IDC and SSC are listed in Table 1, respectively.

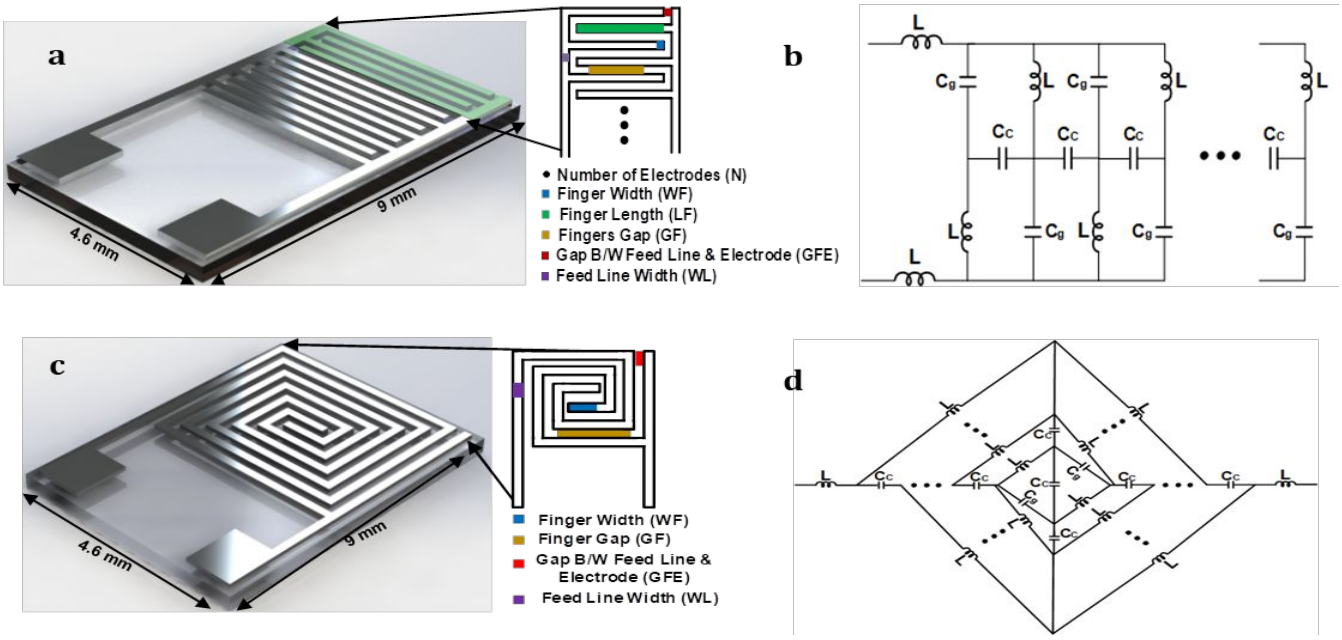

Figure 1 a 3-D schematic with dimension marker of glass substrate based IDC structure b the equivalent circuit of glass substrate based IDC structure c 3-D schematic with dimension marker of square spiral capacitor structure, and d the equivalent circuit of square spiral capacitor structure.

Table 1 Detailed physical parameters of IDC and SSC

	N	LF (μm)	WF (μm)	GF (μm)	GFE (μm)	WL (μm)
SSC	2	41000	100	100	100	100
IDC-1	20	3.8	100	150	100	100
IDC-2	24	3.8	100	100	100	100
IDC-3	32	3.8	100	50	100	100

* SSC represents Squared Spiral Capacitor, * IDC represents Inter-digital Capacitor

Fabrication Process

The right steps and good method play a vital role to fabricate low loss and high-quality devices. The fabrication process for all IDCs and SSC as follow: First, a 6-inch glass wafer was taken and carefully cleaned with acetone, Iso-Propyl Alcohol (IPA), and DI water, respectively. Afterwards, the plasma-enhanced chemical vapour deposition process was used to deposit a silicon nitride (SiN_x) layer. This layer was deposited to increase the adhesion between the glass wafer and the first seed metal layer. Later, first seed metal (Ti/Au) layer was collected through a sputtering process. Subsequently, the desired structure was patterned on a glass wafer through a photolithography process. Photolithography process was performed to achieve a desired height and shape of seed metal with excellent aspect ratio. Later, the seed metal layer was further deposited through the electroplating process. Afterwards, the liftoff process was performed to strip-off the undesired photo-resist (PR) with acetone/IPA/DI, respectively. Lastly, reactive ion etching was done to remove the undesirable seed metal layer from the wafer. The whole fabricated process from simulation to fabrication is shown in Figure S1.

Results and Discussion

Surface Morphology of Aerosol Deposited $BaTiO_3$ Film

The TEM measurement is performed to observe the structural formation and grain density of sensing material at different layers. The cross-sectional view of sensing material prepared at room temperature and annealed at 400 ºC is presented in Figure 2(a). The white and black spots in the figure indicate the availability of grain voids and deposited grain, respectively. The TEM image (Figure 2(a)) reveals the bottom

layer has more grain density than the upper layer. This formation is caused due to the bombarding of high-speed $BaTiO_3$ particles on a glass substrate. The hammering effect on $BaTiO_3$ particles increases grain densification at the bottom layer. The TEM image (Figure 2(b)) indicates the thermal exposure of $BaTiO_3$ film improve surface defect, increase grain size and create uniformity in both layers. The increased grain size improve the ferroelectric property and effective permittivity of deposited $BaTiO_3$ film.[28]

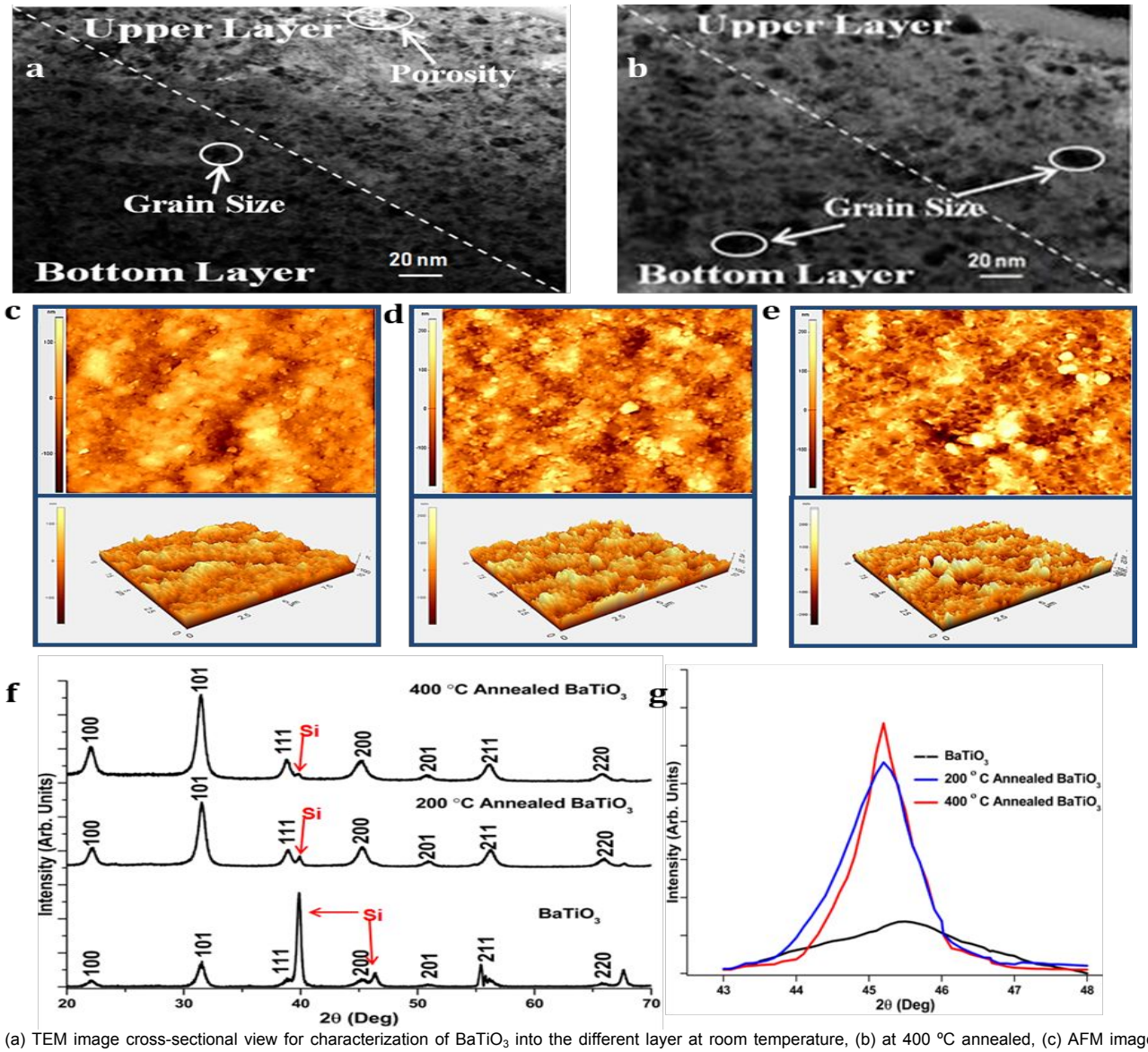

Figure 2 (a) TEM image cross-sectional view for characterization of $BaTiO_3$ into the different layer at room temperature, (b) at 400 ºC annealed, (c) AFM image of $BaTiO_3$ at room temperature, (d) at 200º C annealed, (e) at 400º C annealed, (f) XRD pattern of $BaTiO_3$ at a different temperature, and (g) peak variation corresponding to reflection at (200) phase plane

Similarly, AFM imaging is performed to identify the surface roughness and water vapours adsorption sites on the material surface. The comparison of surface morphology among $BaTiO_3$ film prepared at room temperature, annealed at 200 ºC and 400 ºC is presented in Figures 2(c, d and e) respectively. The surface roughness of deposited $BaTiO_3$ film prepared at room temperature, annealed at 200 ºC and 400 ºC is indicated by the RMS value of 39.7 nm, 52.01 nm, and 65.5 nm, respectively. The high RMS value reveals more adsorption sites for water molecules, enhancement of surface microcracks, and formation of microcapillary sites on sensing material surface. Additionally, the post-annealing of sensing material also enhances water vapour adsorption, desorption sites and attribute high-speed electron transfer. The generation of high-speed electrons is responsible for short response and recovery time.[13]

Crystalline Growth of Aerosol Deposited $BaTiO_3$ Film

The prepared $BaTiO_3$ film is undergoing through shock-load solidification and hammering effect during AD process. This film formation is responsible for small grain size, high

residual stress, and distorted lattice structures. The degraded material properties ascribe low dielectric constant, high leakage current and weak crystalline property of the material.[29] The XRD patterns of aerosol deposited $BaTiO_3$ film prepared at room temperature, annealed at 200 ºC, and 400 ºC are shown in Figure 2(f). The measurement results revealed that the intensity of perovskite peaks are increased with thermal exposure of deposited sensing material. The paraelectric cubic-tetragonal phase plane at 200~45.35º is presented in Figure 2(g). The comparison results indicate the peak phase plane is shifted towards lower angle after thermal treatment of sensing film. This observation attributes the transformation of crystal structure from the cubic phase to the tetragonal phase. The angle shift in the phase plane occurs due to thermal lattice expansion, internal residual stress improvement and crystallization of $BaTiO_3$ film. Additionally, the peak intensity and grain size are also increased after annealing of $BaTiO_3$ at 200 ºC and 400 ºC. The calculated crystal size of $BaTiO_3$ prepared at room temperature, annealed at 200 ºC, and 400 ºC is calculated as 9 nm, 12 nm and 14 nm, respectively.

Humidity Sensing Measurement

The capacitance of proposed IDCs and SSC were calculated using an impedance analyzer (HIOKI IM 3536), which was further connected to the fabricated humidity sensors by coaxial line to record the real-time capacitive variations. The entire measurement process was recorded with the assistance of Labview platform. The phase and voltage of the impedance analyzer were set at 1 MHz and 1 Volt, respectively. The fabricated sensors were tested in a closed humidity chamber (PDL-3J, ESPEC Corp., Japan) by varying the relative humidity (ΔRH) from 30% to 90% for better result characterization. The measurement results of capacitive type humidity sensors are shown in Figure 3 and the sensitivity results presented in Table S2 is calculated as:-

$$\text{Sensitivity } (S) = \frac{\Delta C}{\Delta RH} \quad (7)$$

Where ΔC represents the change in capacitance, and ΔRH represents the change in relative humidity.

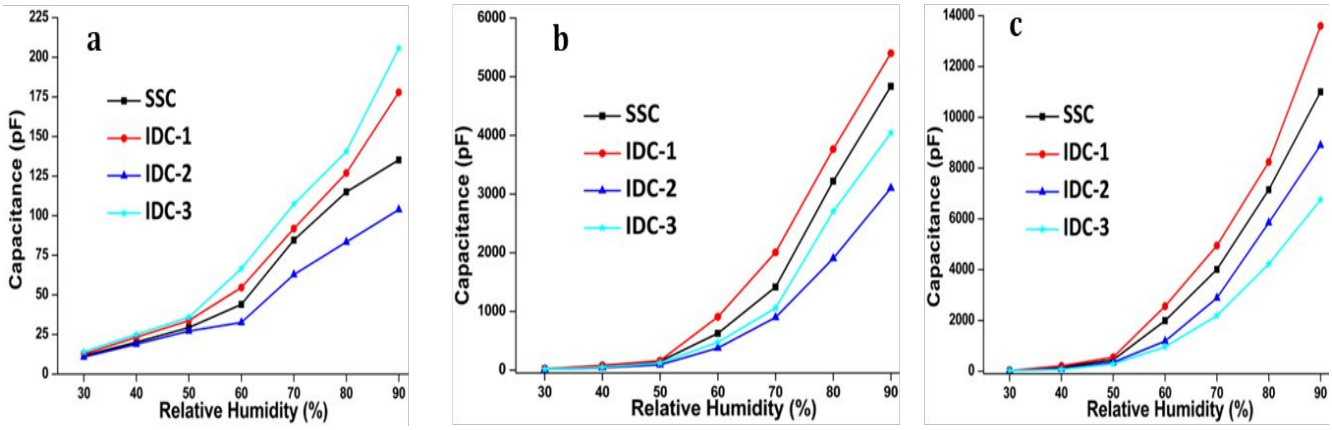

Figure 3 Capacitive type humidity measurement in different design at (a) room temperature, (b) 200 ºC annealed $BaTiO_3$, and (c) 400 ºC annealed $BaTiO_3$

Crystalline Growth of Aerosol Deposited $BaTiO_3$ Film

Measurement result analysis of $BaTiO_3$ film prepared at room temperature. The humidity sensing result of all proposed devices embedded with $BaTiO_3$ film prepared at room temperature is presented in Figure 3(a). The obtained results indicate low sensitivity in all tested method with the rise of RH value form 30% to 90%. The small change in sensitivity is due to the existence of low water adsorption sites, more leakage current and high grain defects in sensing film. The calculated sensitivity result is presented in Table S2 indicate the proposed device (IDC-3) represents high sensitivity at high as well as low RH points. The presence of high sensitivity is due to the minimum gap between adjacent charge electrodes. However, IDC-1 indicates better sensitivity as compared to SSC and IDC-2 due to the presence of high OAR. The high OAR allocates large interaction region for surface deposited water vapours and fringing electric field. However, the interaction of fringing electric field induces significant dissociation of $BaTiO_3$ ions and water molecules. This dissociation conducts ions transportation and increases overall conductivity of deposited sensing film.

Additionally, in a humid environment, the existed water vapours interact with sensing material and create bonding with vacant ions to form the Grotthus chain reaction. These bonding increase ionic conductivity and effective permittivity of sensing material. The enhancement of ionic conductivity and effective permittivity is depended upon the water vapours content at a specific relative humidity level that correspondingly upsurges the device capacitance.

Measurement results analysis of annealed $BaTiO_3$ film at 200 ºC and 400 ºC. Thermal exposure of prepared sensing film dramatically enhances the sensitivity of fabricated devices as presented in Table S2. Thermal treatment minimizes the grain defects, enhance grain to grain connectivity, and increase water

vapours adsorption sites. Annealing effect also reduces oxygen ions (O^{2-}) and generates conduction electrons in $BaTiO_3$ film. These conduction electrons hop between Ti^{3+} and Ti^{4+} ions and decrease the overall grain resistance of deposited material. Additionally, in a humid environment, the thermally excite electrons interact with electric field lines and polarize along with water vapour ions. This alignment of water vapour ions along with thermally excite electrons increases complex effective permittivity of sensing film.[30] The capacitive measurement result and calculated sensitivity of annealed sensing material at 200 ºC are shown in Figure 3(b) and Table S2, respectively. The obtained result indicates the IDC-1 with high OAR represents high sensitivity among all tested devices. Also, the sensitivity result of SSC surpasses IDC-2 and IDC-3 after deposition of annealed sensing material. The high sensitivity of SSC is due to the presence of highly concentrated electric field intensity that polarizes thermally excited $BaTiO_3$ ions and increases material surface energy. The presence of high surface energy at sensing film surface attracts more water molecules to form neutralization.[31] Moreover, the high electric field intensity also creates nucleation of water vapours via Joule heating and convert them into tiny droplets. These tiny water droplets, decrease potential difference and increase the conductivity of deposited material.[32] The agglomeration of water vapours and high surface current increase device sensitivity at high RH points. This observation concludes that the highly concentrated electric field intensity and large OAR are equally responsible for the high sensitivity in SSC and IDC-1, respectively. Furthermore, the capacitance measurement result and calculated sensitivity of fabricated capacitive devices with annealed sensing material at 400 ºC are shown in Figure 3(c) and Table S2. The obtained results indicate, the sensitivity of IDC-2 surpasses the sensitivity of IDC-3 at high as well as low RH points. Additionally, the exponential rise in IDC-2 sensitivity result at high RH points is due to high OAR and the existence of high mesoporous adsorption sites.

Response and recovery time measurement of $BaTiO_3$ film. The obtained results (Table S3) indicate the tested devices embedded with room temperature prepared $BaTiO_3$ film exhibit longer response and recovery time. The generation of extended response and recovery time is due to the non-uniform material structure and high grain defects. These degradations are occurred due to the shock load solidification and hammering effect of prepared $BaTiO_3$ film. The non-uniformed inner structures introduce long-distance for ions to complete reaction whereas, high grain defects hindered dehydration process and ascribe high leakage current that leads to longer reaction/response time.[14] Post annealing is an efficient way to improve response and recovery time in all proposed devices. The proposed sensors decorated with annealed $BaTiO_3$ film exhibits short response and recovery time. Thermal treatment also promotes surface grain expansion and defect filling, resulting in better flatness.[33] These improved defects provide a smooth and faster path for ions to complete their chemical reactions. However, the $BaTiO_3$ film annealed at 400°C represents a slightly longer response and recovery time due to the presence of high open pore ratio that attracts more water molecules toward material surface before saturation.[16] The enhanced adsorption capacity of sensing material increases device sensitivity with a slightly longer response and recovery time in a humid environment.

Electric Field Effect on Sensing Mechanism

The sensitivity analysis of the capacitive sensors is related to the variation of capacitance at different RH points. The complex surface capacitance $\hat{C}_s$ of inter-digital capacitors is proportional to the complex effective permittivity of sensing material and electric field distribution on sensing device defined as[17]

$$\hat{C}_s = \frac{\varepsilon^*_{sm}\hat{E}_z}{V_p} \quad (8)$$

Where, $\hat{E}_z$ represents electric field intensity at z-direction, V_p represents applied voltage potential. At ac input, the complex effective permittivity (ε^*_{sm}) of lossy sensing material can be described as[18]

$$\varepsilon^*_{sm} = \varepsilon + j\left(\frac{\sigma}{\omega}\right) \quad (9)$$

Where, ε represents material relative permittivity, σ represents material surface conductivity, and ω represents wave frequency. The Eq 8 represents the capacitance effect of the inter-digital structure is directly proportional to the electric field intensity in an enclosed volume.

$$C \propto \iiint E\, dv \quad (10)$$

Eqs 8 and 10 indicate the variation of electric field intensity is fully responsible for the change of device capacitance. Moreover, the electric field intensity also affects the properties of ferroelectric material ($BaTiO_3$) used as a sensing layer. Whenever the electric field intensity interacts with $BaTiO_3$, it excites the ions through high interfacial polarization. Basically, in $BaTiO_3$ material structure, Ba ions are very large as compare to Ti ions and form large octahedral interstitial structures. The small Ti ions are unable to position at a stable state inside these octahedral structures and shift themselves off-centred to create an electric dipole. When an electric field interacts with off-centred Ti ions, it alters them from a random position to aligned position with a high degree of polarization. These polarized Ti ions increase the dielectric constant of $BaTiO_3$ film.[17] Similarly, in a humid environment, two vital factors involve to increase device sensitivity through the interaction of the electric field with $BaTiO_3$ sensing layer. First, the vigorous electric field intensity polarizes the water vapour molecules along with Ti ions and uplift the overall complex permittivity of sensing material.[23] Second, the intense electric field lines increase surface energy and decrease water droplet volume deposited on $BaTiO_3$ film. The high surface charge and low droplet volume attract more

water molecules toward $BaTiO_3$ surface. This agglomeration of water molecules on sensing material surface increases complex permittivity, and device sensitivity at high RH points.[32]

Open Area Ratio Effect on Sensing Mechanism

The device structural analysis on the basis of open area ratio is important for the optimization of best geometrical parameters for humidity sensor. In the current section, the variation of device capacitance with the variation of finger gap is discussed. The relationship present in Eqs. 5 and 6 indicate that the fabricated device capacitance increases when the complex permittivity of sensing material increases and decrease when the finger gap of adjacent charge electrodes increases as:-

$$C_{IDC}\ or\ C_{ssC} \propto \varepsilon^*_{sm} \frac{WF \times LF}{GF} \quad (11)$$

The penetration depth of fringing electric field lines is proportional to the gap between adjacent charge electrodes [19]. The conceptual schematic view of penetrated electric field lines in the inter-digital structure is shown in Figures 4 (a_i, a_{ii}, a_{iii}).

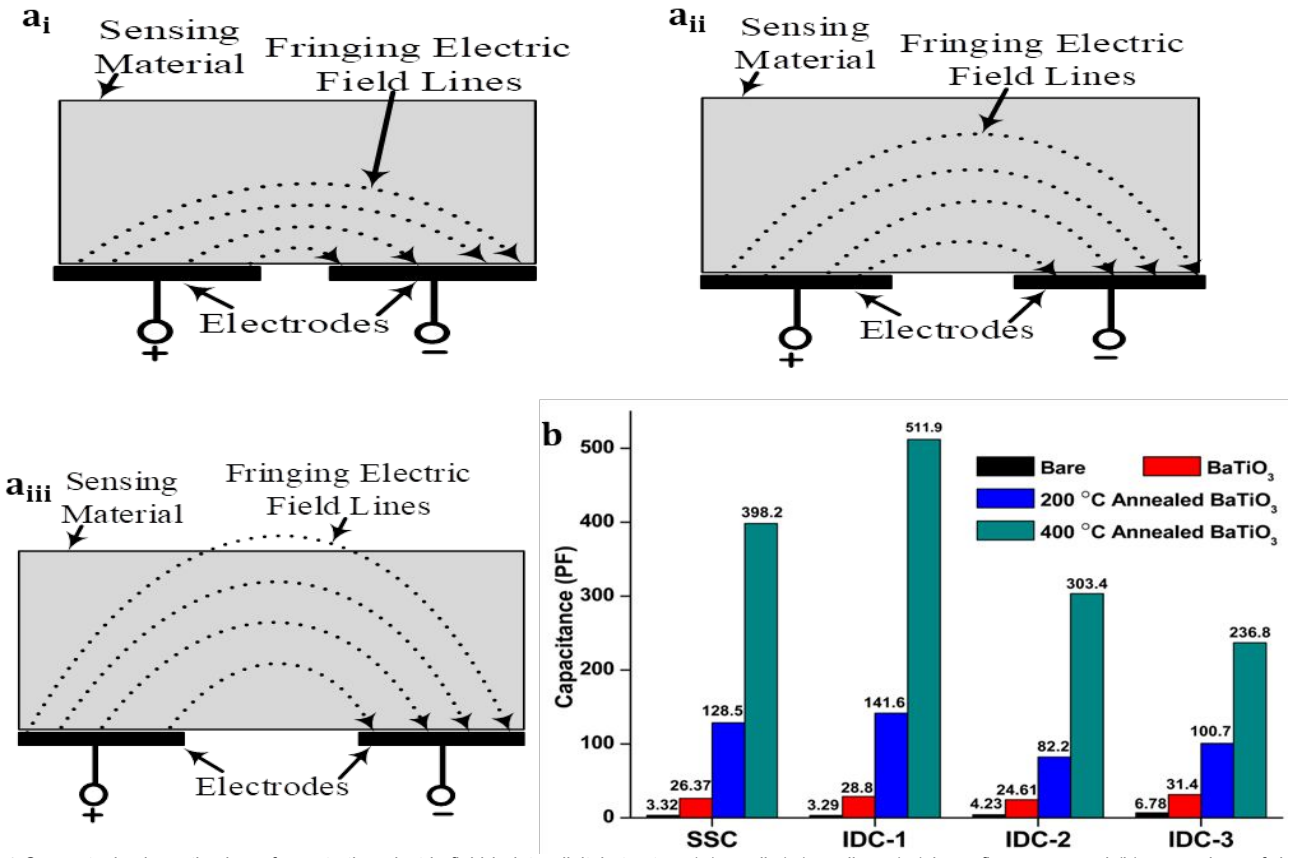

Figure 4 Conceptual schematic view of penetrating electric field in inter-digital structure (a_i) small, (a_{ii}) medium, (a_{iii}) large finger gap, and (b) comparison of design capacitance with variation in sensing material temperature

The large distance between adjacent charge electrodes, increase the interaction area of electric field intensity and sensing layer. However, the electric field intensity is inversely proportional to the distance between adjacent charges electrodes shown in Figure S2 and represented as[19]

$$Electric\ field\ (E) = \frac{Applied\ Voltage\ (V)}{GF} \quad (12)$$

The gap between adjacent charge electrodes of SSC, IDC-1, IDC-2, and IDC-3 is 100 µm, 150 µm, 100 µm and 50 µm, respectively. Among all fabricated IDCs, IDC-3 with minimum finger gap represents high electric field intensity at the bare condition. Additionally, the fabricated SSC structure with 100 µm finger gap induces high electric field intensity due to long length circular electrodes. The continuous flow of surface electric current and mutual coupling between adjacent charge electrodes are responsible for highly concentrated electric field intensity. The presented Figures 4(a_{iii}) and S1 conclude that the device (IDC-1) with 150 µm finger gap generates minimum electric field intensity, but introduces a large area of interaction in sensing material. The OAR analysis is performed to verify the theoretical concept of optimized design structure. OAR represents the ratio of the non-conductive and conductive region present in material deposition area of the device, represented in Table S1. The OAR of SSC, IDC-1, IDC-2, and IDC-3 is calculated as 49.8%, 56.9%, 47.8%, and 32.68%, respectively. The capacitive measurement of all devices is performed in an open air environment at bare condition, with $BaTiO_3$ film prepared at room temperature and post-annealed

$BaTiO_3$ film (at 200 ºC and 400 ºC) as shown in Figure 4(b). At bare condition, IDC-3 indicates high capacitance due to the minimum gap between adjacent charge electrodes. Similarly, after the deposition of room temperature prepared $BaTiO_3$ film, the capacitance of IDC-1 with 150 µm gap is surpassed the capacitance of SSC and IDC-2, but still lower than IDC-3. The lower capacitance of IDC-1 is due to the high surface defect, non-uniform structure and existence of less water adsorption sites in prepared material. In an open environment, the presence of water vapour open quickly saturates the sensing material with less water adsorption site and ceases all fabricated devices at low capacitance. The thermal treatment of $BaTiO_3$ film introduces high electrons density, enhanced of grain to grain connectivity, improved surface defect and the existence of more water vapour adsorption sites on the material surface. These improvements of sensing material property enhance the capacitance of all fabricated devices. After post-annealing, IDC-1 with 150 µm finger gap demonstrates high capacitance value among all tested devices. The high capacitance is achieved due to the presence of a wider interaction region for fringing electric field lines and deposited water vapour on sensing material. The wider interaction area allows more water vapour ions to be polarized and generate high capacitance in measuring devices. Additionally, the tested SSC device presents higher capacitance than IDC-2 in spite of almost identical finger gap. This enhancement is due to the presence of a highly concentrated electric field in the SSC device structure as represented in Figure S3.

Sensing Material Effect on *$BaTiO_3$ film*

Ionic conduction model for *$BaTiO_3$ film*. The interaction of water vapours with $BaTiO_3$ layer induces protonation that escalates conductivity and relative effective permittivity of sensing material. The induced protonation generates quick and rapid movement of H^+ ions towards the cathode and OH^- ions towards the anode. The movement of OH^-, H^+, H_3O^+, Ba^{2+}, and TiO_3^{2-} ions are responsible for high ionic conductivity.[9] The interaction of water molecules with $BaTiO_3$ layer can be well explained through iconic conduction model presented in Figure S4.

Annealing effect on humidity *$BaTiO_3$ film*. Humidity-sensing properties are co-determined by the susceptibility of materials surfaces to hydration, inner and surface microstructures. Moderate thermal treatment could improve these properties, whereas more or less thermal effects might cause an inferior case. The annealing effect on humidity sensing film is explained as follow:-

$BaTiO_3$ crystal properties promotion. During the AD process, $BaTiO_3$ particles underwent two-step fragmentation. First, ascribe to the effect of shock-loading solidification and second attributes to the hammering effect of subsequent deposition of high-speed particles. The dual fragmentation of $BaTiO_3$ film results in residual stress and crystal structure distortion. These defects severely affect the grain crystal property of deposited film and make it more susceptible to hydration.[12] The high-temperature treatment is a promising solution to relieve the residual stress and crystal distortion that further enhance the susceptibility of $BaTiO_3$ grains toward hydration

Surface hydrophilicity enhancing. A large amount of nano-scale grains and crevices are favourable to improve surface hydrophilicity.[34] The thermal treatment further promotes the surface grain expansion and defect filling that results in better flatness and higher H/L.[14] Additionally, the 400 °C treatment with the more thermal effect caused a higher surface roughness and presents more hydrophilicity over 200 °C case.

Inner microstructure adjustment. The 400 °C treatment of $BaTiO_3$ film induces a thermal solid-phase reaction and transforms the internal structure from a non-uniform to a uniform state. These improvements of inner structure improve the dielectric properties and enhance humidity absorption capacity of sensing film. The initial film structure determines the required heating time, and the temperature wherein a non-uniformed inner structure needs a long distance to complete this reaction. After a series of experiments, 400°C treatment for 2 h was identified as the superior option.[14]

Protonic effect. Thermal treatment of $BaTiO_3$ induces oxygen ions (O^{2-}) reduction and generates conduction electrons. These conduction electrons hop between Ti^{3+} and Ti^{4+} ions and decrease the overall grain resistance of deposited $BaTiO_3$ film. Additionally, in a humid environment, the thermally excite electrons interact with the induced electric field and polarized along with water vapour ions. These alignments of water vapour ions along with thermally excited electrons increases complex permittivity of sensing film.[30]

Hygroscopic film effect on humidity sensing

The implementation of the AD method to deposit sensing material on a glass substrate is responsible for the generation of multi-dielectric $BaTiO_3$ layer. The surface morphology of the aerosol $BaTiO_3$ layer indicates high material destiny of bottom layer compared to the upper layer due to the bombarding of $BaTiO_3$ precursor on the glass substrate. It is assumed that the deposited $BaTiO_3$ has relatively high complex permittivity at the bottom layer as compared to the upper layer ($\varepsilon_{up}^* < \varepsilon_{Bot}^*$). Since the fabricated devices are based on IDC structure having internal and external electrodes. So the overall capacitance after multi-dielectric layer deposition based on internal and external electrodes can be expressed as.[35]

$$C_i = LF\left[\left(\varepsilon_{Bot}^* - \varepsilon_{up}^*\right)k_i^c(\eta,r) + \varepsilon_{air}k_i^c(\infty)\right] \quad (13)$$

$$C_e = LF\left[\left(\varepsilon_{Bot}^* - \varepsilon_{up}^*\right)k_e^c(\eta,r) + \varepsilon_{air}k_e^c(\infty)\right] \quad (14)$$

Also, $k_i^c(\infty) = \sin\left(\frac{\eta\pi}{2}\right)$ and $k_e^c(\infty) = \frac{2\sqrt{\eta}}{1+\eta}$ (15)

Where k_i^crepresents interior electrode-based unit cell constant, k_u^c represents exterior electrode-based unit cell constant, η represents metallization ratio, and r represents as height to width ratio. The metallization ratio and height to width ratio can be evaluated as

$$\eta = \frac{WF}{WF+GF} \quad (16)$$

$$r = \frac{2h}{WF+GF} \quad (17)$$

Where *h* represents the height of the sensing layer. The presented Eqs (13) and (14) reveal that the capacitance variation of the overall inter-digital structure is proportional to the overall permittivity of sensing material and the finger gap between adjacent electrodes. Moreover, the complex permittivity of the bottom layer has actively interacted with high electric field interaction and further responsible for high sensitivity.

Temperature effect on humidity sensing

Temperature effect on humidity chamber air. The temperature can affect the humidity sensing performance by changing the dew point temperature value of atmospheric air. Moreover, at high temperature, ambient air can hold more water vapours and decrease atmospheric relative humidity value. The warmer air can able to store more water vapours Before reaching a saturation point due to the existence of high dew point temperature value.[36] The high dew point temperature value demands more water vapours to indicate the existence of specific relative humidity in the environment. This enhancement of water vapour density affects the sensing performance of the humidity sensor at different relative humidity points.[37]

Temperature Effect on the capacitance of proposed devices. The temperature variation can effects the capacitance of the capacitive sensor as represent in Eq (18)[38] :

$$C = \frac{\varepsilon_0 \varepsilon_{sm}^*}{d} \exp\left[-\frac{\phi}{kT}\right] \quad (18)$$

Where *d* represents the distance between adjacent charge electrode, ϕ represents activation energy of $BaTiO_3$, *K* represents Boltzmann constant ($K = 1.38 \times 10^{-23} J/K$) and *T* represents temperature in kelvin. Above equation indicates the rise in temperature exponentially increase the capacitance value of a capacitive sensor.[12]

The obtained result of proposed humidity sensors is compared with several previously reported capacitive humidity sensors, as presented in Table 2. The analyzed results indicate that the proposed inter-digital devices exhibit high sensitivity and short response/recovery time. Also, the post-annealing $BaTiO_3$ film at 400 °C reveals high sensitivity due to a reduction in grain defects, enhancement of grain to grain connectivity, and an increase in water vapours adsorption sites.

Table 2 Performance comparison of the different capacitive type humidity sensor

Device Type	Material	Preparation technique	Annealing Process	Sensitivity	Res/Rec	Ref.
MIM	BaTiO3 powder	Cold Isostatic Sintering	1 h at 600 °C	154	15 s/ 250 s	6
IDC	BaTiO3 powder	Screen Printing	0.5 h at 600−650 °C	140.00	N.A.	7
IDC	BaTiO3 sol−gel	Spin Coating	1 h at 600 °C	148.33	30 s/ 40 s	9
IDC	BaTiO3 sol−gel	Electrospinning	2 h at 800 °C	214.21	4 s/ 5 s	13
IDC	BaTiO3 powder	Aerosol Deposition	2 h at 400 ◦C	171.04	3 s/ 5 s	16
IDC	BaTiO3 powder	Aerosol Deposition	Room Temperature	3.19 (IDC-3)	12 s/ 15s	This work
IDC	BaTiO3 powder	Aerosol Deposition	2 h at 200 °C	89.61 (IDC-1)	4s/ 5s	
IDC	BaTiO3 powder	Aerosol Deposition	2 h at 400 °C	226.33 (IDC-1)	5 s/ 7s	

* Res/Rec represents Response Time/Recovery Time and s* represents second

Conclusion

In this article, ultra-high sensitive AD prepared $BaTiO_3$ film loaded IDCs, and an SSC is proposed for humidity sensing application. The deposited $BaTiO_3$ film is prepared at room temperature, then post-annealed at 200 ºC and 400 ºC to improve its sensing properties. The sensitivity analysis is demonstrated by capacitive variation of fabricated devices at different RH points. The obtained results indicate the precise selection of post-annealing temperature, high electric field intensity and large OAR are the vital factor in achieving high sensitivity in $BaTiO_3$ based humidity sensor. The interaction of concentrate electric field intensity with the surface deposited water vapours induces protonation and polarization of ions thus increase in complex effective permittivity of sensing material. The enhancement of complex effective permittivity depends upon the water vapours content present in the humid air. The fabricated IDC-1 with high OAR indicates exponential sensitivity enhancement, after deposition of annealed sensing material. Additionally, the fabricated SSC device presented high sensitivity due to the involvement of concentrated electric field intensity and high OAR. The current study reveals that the design structure, electric field interaction and sensing material quality are equally responsible for high sensitivity in capacitive humidity sensors.

Acknowledgement

This work was supported by the General Financial Grant from the China Postdoctoral Science Foundation (2017M611367), Heilongjiang Postdoctoral Fund (LBH-Z17056), Fundamental Research Fund for the Central Universities, and sponsored by Zhejiang Lab (2019MC0AB03).

References

(1) Farahani, H.; Wagiran, R.; Hamidon, MN. Humidity Sensors Principle, Mechanism, and Fabrication Technologies: A Comprehensive Review. *Sensor.* **2014,** 14, 7881−7939. https://doi.org/10.3390/s140507881

(2) Rahim, I.; Shah, M.; khan, A.; Luo, J.; Zhong, A.; Li, M.; Ahmed, R.; Li, H.; Wei, Q.; Fu, Y. Capacitive and resistive response of humidity sensors based on graphene decorated by PMMA and silver nanoparticles, *Sens. and Act.-B.* **2018,** 267, 42-50. https://doi.org/10.1016/j.snb.2018.03.069

(3) Subbarao, N. V. V.; Gedda, M.; Iyer, P. K.; Goswami, D. K. Organic field-effect transistors as high-performance humidity sensors with rapid response, recovery time and remarkable ambient stability, *Org. Elect.* **2016**, 32, 169-178. https://doi.org/10.1016/j.orgel.2016.02.017

(4) Gu, L.; Huang, Q.A.; Qin, M. A novel capacitive-type humidity sensor using CMOS fabrication technology, *Sens. and Act.-B,* **2004,** 99, 491-498. https://doi.org/10.1016/j.snb.2003.12.060

(5) Urbiztondo, M.; Pellejero, I.; Rodriguez, A.; Pina, M. P.; Santamaria, J. Zeolite-coated interdigital capacitors for humidity sensing, *Sens. and Act.-B*, **2011,** 157, 450–459. https://doi.org/10.1016/j.snb.2011.04.089

(6) Viviani, M.; Buscaglia, M. T.; Buscaglia, V.; Leoni, M.; Nanni, P. Barium Perovskites as Humidity Sensing Materials, *J. Euro. Cer, Soc.* **2001,** 21, 1981–1984. https://doi.org/10.1016/S0955-2219(01)00155-8

(7) Wang, J.; Wang, X. H.; Wang, X. D.; Study on dielectric properties of humidity sensing nanometer materials, *Sens. and Act.-B,* **2005,** 108, 445–449. https://doi.org/ 10.1016/j.snb.2004.11.089

(8) Yamazoe, N.; Shimizu, Y. Humidity Sensors: Principles and Application, *Sens. and Act.-B,* **1986,** 10, 379–398. https://doi.org/10.1016/0250-6874(86)80055-5

(9) Yuk, J.; Troczynski, T. Sol–gel $BaTiO_3$ Thin Film for Humidity Sensors, *Sens. and Act.-B,* **2003,** 94, 290–293. https://doi.org/10.1016/S0925-4005(03)00371-X

(10) Wang, L.; Hea, Y.; Hua, J.; Qia, Q.; Zhanga, T. DC Humidity Sensing Properties of $BaTiO_3$ Nanofiber Sensors with Different Electrode Materials, *Sens. and Act.-B,* **2011,** 153, 460–464. https://doi.org/10.1016/j.snb.2010.11.016

(11) Farea, A. M.; Kumar, S.; Batoo, K. M.; Yousef, A.; Lee, C. G. Influence of the Doping of Ti_4^+ Ions on Electrical and Magnetic Properties of $Mn_{1+x}Fe_{2-2x}Ti_xO_4$ Ferrite. *J. Alloys and Comp,* 2009, 469, 451−457. https://doi.org/10.1016/j.jallcom.2008.01.139

(12) Li, X.; Qiu, F.; Guo, K.; Zou, B.; Gu, J.; Wang, J.; Xu, B. Synthesis and Humidity Sensitive Properties of Nanocrystalline $Ba_{1-x}Sr_xTiO_3$ Thick Films, *Mat. Chem. and Phy.* **1997,** 50, 227−232. https://doi.org/10.1016/S0254-0584(97)01938-X

(13) He, Y.; Zhang, T.; Zheng, W.; Wang, R.; Liu, X.; Xia, Y.; Zhao, J. Humidity Sensing Properties of $BaTiO_3$ Nanofiber Prepared via Electrospinning, *Sens. and Act.–B.* **2010,** 146, 98−102. https://doi.org/10.1016/j.snb.2010.02.030

(14) Liang, J. G.; Wang, C.; Yao, Z.; Liu, M. Q.; Kim, H. K.; Oh, J. M.; Kim, N. Y. Preparation of Ultrasensitive Humidity-Sensing Films by Aerosol Deposition, *ACS App. Mat. Inter.* **2018,** 10, 851−863. https://doi.org/ 10.1021/acsami.7b14082

(15) Oikonomou, P.; Manoli, K.; Goustouridis, D.; Raptis, I.; Sanopoulou, M. Polymer/$BaTiO_3$ nanocomposites based chemocapacitive sensors, *Microelect. Eng.* **2009,** 86, 1286–1288. https://doi.org/10.1016/j.mee.2008.11.081

(16) Liang, J. G.; Kim, E. S.; Wang, C.; Cho, M. Y.; Oh, J.; Kim, N. Y. Thickness effects of aerosol deposited hygroscopic films on ultra-sensitive humidity sensors, *Sens. and Act.-B.* **2018,** 265, 632–643. https://doi.org/10.1016/j.snb.2018.03.093

(17) Mamishev A. V.; Sundara, R. K.; Yang, F.; Du, Y. Q.; Zahn, M. Inter-digital sensors and transducers, *Proc. IEEE.* **2004,** 92, 808–845. https://doi.org/10.1109/JPROC.2004.826603

(18) Grimnes, S.; Martinsen, O. G. Bioimpedance and Bioelectricity Basics, Third ed., *Academic Press*. **2015**, 37-75.

(19) Prasad, K. D.; Electromagnetic Field and Waves, *Satya Prakashan.* **2001**, 85-247.

(20) Khalfallaoui, A.; Burgnies, L.; Blary, K.; Velu, G.; Lippens, D.; Carru, J. C. Downscaling at Submicrometer Scale of the Gap Width of Interdigitated $Ba_{0.5}Sr_{0.5}TiO_3$ Capacitors, *IEEE Trans. on Ultras. Ferro. and Freq. Contr.* **2015,** 62, 247-254. https://doi.org/10.1109/TUFFC.2014.006639

(21) Nayak, S.; Chaki, T. K.; Khastgir, D. Development of Flexible Piezoelectric Poly (dimethylsiloxane) − $BaTiO_3$ Nanocomposites for Electrical Energy Harvesting, *Ind. and Eng. Chem. Res.* **2014,** 53, 14982−14992. https://doi.org/10.1021/ie502565f

(22) Lausser, C.; Zahn, D.; Colfen, H. Barium Titanate Nanoparticle Self-Organization in an External Electric Field, *J Mat. Chem.* **2011,** 21, 16978−16982. https://doi.org/10.1039/C1JM13061G

(23) He, D. Y.; Qiao, L. J.; Khodayari, M.; Volinsky, A. A. Electric field and humidity effects on adsorbed water behavior on $BaTiO_3$ ferroelectric domains studied by scanning probe microscopy, *J. App. Phy.* **2014,** 116, 084105(1-9). https://doi.org/10.1063/1.4894006

(24) Baek, E.; Yun, Y. S.; Kim, H. K.; Lee, S. H.; Lee, S. G.; Im, I. H.; Lee, Y. H. Effect of Post-Annealing on $(Ca_{0.7}Sr_{0.3})(Zr_{0.8}Ti_{0.2})O_3$ Films on Pt and Cu Substrates Fabricated by Aerosol Deposition, *J. Nano. and Nanotech.* **2015,** 15, 8478−8483. https://doi.org/ 10.1166/jnn.2015.11453

(25) Chuluunbaatar, Z.; Adhikari, K. K.; Wang, C.; kim, N. Y. Micro-Fabricated Bandpass Filter using Intertwined Spiral Inductor and Interdigital Capacitor, *Elect. Lett.* 2014, 50, 1296–1297. https://doi.org/10.1049/el.2014.2040

(26) Huang, F.; Lu, J.; Jiang, N. Scalable Distributed-Capacitance Model for Silicon On-Chip Spiral Inductors, *Micro. and Opt. Tech. Lett.* **2006,** 48, 1423-1427. https://doi.org/10.1002/mop.21642

(27) Lee, K. H.; Kim, E. S.; Liang, J. G.; Kim, N.Y.; Design and Realization of a Compact High-Frequency Band-Pass Filter with Low Insertion Loss Based on a Combination of a Circular-Shaped Spiral Inductor, Spiral Capacitor and Interdigital Capacitor, *Elect.* **2018,** 7, 195(1-7). https://doi.org/10.3390/electronics7090195

(28) Hoshina, T.; Furuta, T.; Kigoshi, Y.; Hatta, S.; Horiuchi, N.; Takeda, H.; Tsurumi, T. Size Effect of Nanograined $BaTiO_3$ Ceramics Fabricated by Aerosol Deposition Method, *Jap. J. App. Phy.* **2010,** 49, 09MC02(1-5). https://doi.org/10.1143/JJAP.49.09MC02

(29) Maie, H. Synthesis and Dielectric Properties of Nanocrystalline Barium Titnate and Silver/Barium Titnate particles, *Dissertation, Clemson University*. **2008.**

(30) Guo, Y.; Batra, S.; Chen, Y.; Wang, E.; Cakmak, M. Roll to Roll Electric Field "Z" Alignment of Nanoparticles from Polymer Solutions for Manufacturing Multifunctional Capacitor Films, *ACS App. Mat. Int.* **2016,** 8, 18471−18480. https://doi.org/10.1021/acsami.6b05435

(31) He, D. Y.; Qiao, L. J.; Volinsky, A. A.; Bai, Y.; Wu, M.; Chu, W. Y. Humidity effects on (001) $BaTiO_3$ single crystal surface water adsorption, *App. Phy. Lett.* **2011,** 98, 062905(1-3). https://doi.org/10.1063/1.3544586

(32) Sareecha, N.; Shah, W. A.; Anis-ur-Rehman, M.; Mirza, M. L.; Awan, M. S. Electrical investigations of $BaTiO_3$ ceramics with Ba/Ti contents under influence of temperature, *Sol. Sta. Ion.* **2017,** 303, 16–23. https://doi.org/10.1016/j.ssi.2017.02.003

(33) Kotnala, R. K.; Shah, J.; Singh, B.; kishan, H.; Singh, S.; Dhawan, S. K.; Sengupta, A. Humidity response of Li-substituted magnesium ferrite, *Sens. Actuators B Chem.* **2008,** 129, 909–914. http://dx.doi.org/10.1016/j.snb.2007.10.002.

(34) Zhu, D.; Fu, Y.; Zang, W.; Zhao, Y.; Xing, L.; Xue, X. Piezo/active humidity sensing of CeO2/ZnO and SnO2/ZnO nano-array nano-generators with high response and large detecting range, *Sens. and Act. B.* **2014,** 205, 12–19. http://dx.doi.org/10.1016/j.snb.2014.08.060

(35) Blume, S. O. P.; Mrad, R. B.; Sullivan, P. E. Modelling the capacitance of multi-layer conductor-facing interdigitated electrode structures, *Sens. and Act.-B.* **2016,** 213, 423–433. https://doi.org/10.1016/j.snb.2015.02.088

(36) www.delmhorst.com/blog/relative-humidity-meter-readings

(37) Wu, Y.; Gu, Z. Metal-Insulator-Semiconductor $BaTiO_3$ Humidity Sensor, *Symp. on Phot. & Optoelect.,* Wuhan, China, **2009**. https://doi.org/10.1109/SOPO.2009.5230200